

A search for variable white dwarfs in large area time domain surveys: a pilot study in SDSS Stripe 82

Nicola Pietro Gentile Fusillo¹, J. J. Hermes¹, Boris T. Gänsicke¹

¹ *Department of Physics, University of Warwick, Coventry, CV4 7AL, UK*

29 October 2015

ABSTRACT

We present a method to reliably select variable white dwarfs from large area time domain surveys and apply this method in a pilot study to search for pulsating white dwarfs in the Sloan Digital Sky Survey Stripe 82. From a sample 400 high-confidence white dwarf candidates, we identify 24 which show significant variability in their multi-epoch Stripe 82 data. Using colours, we further selected a sample of pulsating white dwarf (ZZ Ceti) candidates and obtained high cadence follow up for six targets. We confirm five of our candidates as cool ZZ Ceti, three of which are new discoveries. Among our 24 candidates we also identify: one eclipsing binary, two magnetic white dwarfs and one pulsating PG1159 star. Finally we discuss the possible causes for the variability detected in the remaining targets. Even with sparse multi-epoch data over the limited area of Stripe 82, we demonstrate that our selection method can successfully identify various types of variable white dwarfs and efficiently select high-confidence ZZ Ceti candidates.

Key words: (stars:) white dwarfs -stars: oscillations: including pulsations - stars: variables: general - surveys

1 INTRODUCTION

Many white dwarfs show some degree of variability in their apparent brightness. These brightness changes can be very different in nature: bright eruptions in interacting binaries (cataclysmic variables or classical novae; Warner 1995), eclipsing binaries (e.g. Green et al. 1978; Orosz & Wade 1999; Parsons et al. 2015), rotationally variable magnetic white dwarfs (Barstow et al. 1995; Brinkworth et al. 2004, 2013; Lawrie et al. 2013), pulsating white dwarfs (Lasker & Hesser 1971; Bergeron et al. 1995; Mukadam et al. 2004; Nitta et al. 2009) and even systems in which the cause of variability is still unexplained (Maoz et al. 2015; Holberg & Howell 2011). Each one of these classes offers a unique and different channel to explore white dwarf structure and evolution. Pulsating white dwarfs, in particular, are extraordinary tools to probe their interior structure.

Traditionally, the physical parameters of white dwarfs, including their effective temperature (T_{eff}) and surface gravity ($\log g$) are determined from spectroscopic analysis (Bergeron et al. 1992). However, spectral information is restricted to the outermost layers of the star. As a consequence, our understanding of white dwarfs is often, literally, superficial.

The existence of pulsating white dwarfs, however, provides a unique opportunity to probe the interior of

these objects. Asteroseismology can be used to investigate the structure, composition and mass of both the core and envelope (Winget & Kepler 2008; Fontaine & Brassard 2008; Althaus et al. 2010), internal rotation profiles (Charpinet et al. 2009), measure weak magnetic fields (Winget et al. 1991) and even search for planetary companions via pulse timing variations (Winget et al. 2003; Mullally et al. 2008). Since most, if not all, white dwarfs evolve through a phase of pulsations as they cool, asteroseismological studies can shed light on the internal structure of the global white dwarf population (e.g. Robinson 1979; Fontaine et al. 1985, 2003; Romero et al. 2012).

Current observational evidence suggests that all hydrogen-atmosphere (DA), while cooling through the temperature range $\simeq 12,500 - 11,000$ K, will undergo global, non-radial pulsations (Bergeron et al. 2004; Gianninas et al. 2011). These pulsating white dwarfs are known as DAV or ZZ Ceti. Aside from ZZ Ceti, there are at least two more classes of pulsating white dwarfs: hot pre-white dwarfs (PG1159 or DOV; McGraw et al. 1979) and helium atmosphere (DB) white dwarfs (V777 Her or DBV; Winget et al. 1982). Recent studies suggested that variable hot carbon atmosphere (DQ) white dwarfs may constitute a further class of pulsators (Fontaine et al. 2008; Montgomery et al. 2008), however the true nature of their variability is still matter of debate (Lawrie et al. 2013).

The first ZZ Ceti and indeed the the first pulsating white dwarf, DA HL Tau 76, was serendipitously discovered in 1965 by Landolt (1968). Since then, approximately 180 similar objects have been identified and today ZZ Ceti are by far the largest and best studied class of pulsating white dwarfs. Their pulsation periods typically range from 100 to 1400 seconds (Clemens 1993; Mukadam et al. 2004) and can reach up to 1.7 hours for extremely low-mass ($M_{WD} < 0.25M_{\odot}$) white dwarfs (Hermes et al. 2013). Historically, unambiguous identification of pulsating white dwarfs required several hours of continuous high cadence photometry (e.g. Mukadam et al. 2004; Nitta et al. 2009), which is observationally expensive. Candidate selection has so far relied on colours and/or T_{eff} and $\log g$, estimated from model fits to spectra, with efficiencies ranging from 30% to 80% (e.g. Mukadam et al. 2004).

In recent years, the opportunity to repeatedly survey large areas of the sky has rapidly advanced the field of time-domain astronomy. Time-domain exploration of the sky is at the forefront of modern astronomy with many wide-field surveys in operation or soon to come on-line (eg. CRTS, Drake 2014; PTF, Law et al. 2009; EVRYSCOPE, Law et al. 2015; Pan-STARRS, Morgan et al. 2014; Gaia, Walton 2014; LSST, Ivezić et al. 2011). In order to fully exploit these vast resources we will need to develop efficient selection algorithms, e.g. a robust method to identify pulsating white dwarf candidates is needed to optimize high-cadence photometric follow-up.

Here, we investigate the feasibility of using multi-epoch photometry from large-area surveys to reliably identify pulsating white dwarf candidates based on Stripe82 of the Sloan Digital Sky Survey (SDSS). Several successful studies have made use of Stripe82 multi-epoch observations to search for variable objects (eg. Sesar et al. 2007; Bramich et al. 2008; Becker et al. 2011). However these studies mainly focused on identifying large-amplitude variable sources (e.g eclipsing binaries or flaring stars) and the potential of identifying low amplitude variability (like that of pulsating white dwarfs) has not yet been explored. Starting from a sample of 400 high-confidence white dwarfs candidates from the catalogue of Gentile Fusillo et al. (2015), we recover, recalibrate and quality-control all available multi-epoch photometry to identify variable candidates. Even though Stripe82 offers only low and irregular cadence over a relatively limited area, our study demonstrates promising results. In the near future a similar methodology, applied to superior time-domain surveys (e.g. Pan-STARRS, Gaia and LSST) will completely change the way we identify high-amplitude variable stars, including pulsating white dwarfs.

2 SDSS STRIPE 82

SDSS has obtained *ugriz* multi-band photometry, in the magnitude range $g \simeq 15 - 22$ mag, for over a third of the sky, and spectroscopic follow up of over 4 million objects (Alam et al. 2015).

A particular region of the SDSS footprint, Stripe 82, has received multiple observations as part of different programs (most notably the SDSS-II Supernova survey, Frieman et al. 2008; Sako et al. 2008). Stripe 82 covers an area of 300 deg^2 on the celestial equator spanning 8 hours in right ascen-

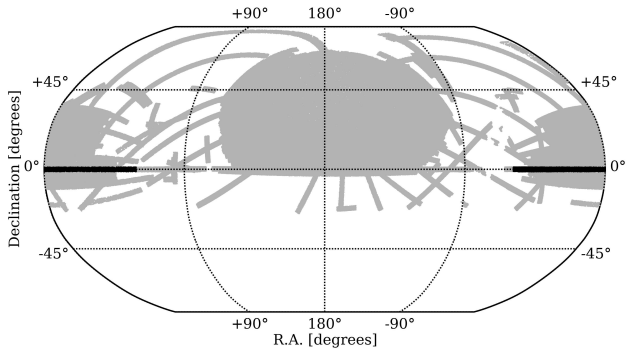


Figure 1. Current photometric footprint of SDSS (data release 12, Alam et al. 2015; $\simeq 14,000 \text{ deg}^2$). The 300 deg^2 of Stripe82 are shown in black.

sion ($-50^\circ < \text{RA} < 59^\circ$) and 2.5 degrees in declination ($-1.25^\circ < \text{Dec} < 1.25^\circ$, see Fig. 1). The stripe consists of two scan regions which have been repeatedly imaged over approximately ten years with a total of 303 imaging runs. A specific imaging run may cover the entire length of the stripe or just a specific region, and several runs overlap in certain areas (Abazajian et al. 2009).

3 DATA SELECTION AND CORRECTION

We retrieved photometry for 400 high-confidence white dwarf candidates from the catalogue of Gentile Fusillo et al. (2015) which fall in Stripe82 and have *probability of being a white dwarf* (P_{WD}) ≥ 0.75 . We found that, on average, each white dwarf had been observed between 60 and 200 times. Only about one-quarter of the Stripe82 scans were obtained in photometric conditions; the rest were taken under variable clouds and often poorer than normal seeing. As a consequence, the default calibration of the Stripe82 photometry is insufficient to identify low-amplitude variables. In fact, all 400 white dwarf candidates (and their neighbouring objects) show significant low-amplitude variability (up to $\simeq 0.2$ mag) in their Stripe82 lightcurves.

In the standard procedure to correct for varying atmospheric conditions in time-series photometry, *relative (or differential) photometry*, simultaneous observations of one or more neighbouring objects are used to calibrate the photometry of the science target. Changing atmospheric conditions affect neighbouring objects in the same way and can therefore be measured and corrected for. We followed this approach using the neighbouring stars of our white dwarf candidates to recalibrate the Stripe82 observations, and identify unreliable detections. For each white dwarf candidate we retrieved Stripe82 photometry of all point sources with “clean” photometry within a five arcminute radius, which were observed at the same time as the white dwarf. We defined an “individual nightly offset” as the difference between the *ugriz* magnitudes of an object as detected on a given night and the median of all Stripe82 measurements of that object. Calculating the median of the “individual nightly offsets” for all neighbours, then defined a “median nightly offset” which we used to correct the Stripe82 magnitude of the white dwarf on that night.

However, several effects (such as irregular cloud cover-

age or intrinsic variability of a neighbour) can cause irregular variations from object to object, hence in certain nights the “individual nightly offsets” are not consistent with each other and can therefore not be used to re-calibrate the field. We compare the “individual nightly offsets” of all neighbours with the “median nightly offset” and calculate reduced χ^2 values. If a significant scatter is observed ($\chi^2_{\text{red}} > 3$) we conclude that the “median night offset” cannot be considered reliable and discard the night. Furthermore we also consider unreliable those nights in which less than four neighbours were observed.

Following this strict selection criteria, 85 of our white dwarf candidates were left with less than eight epochs of reliable data, which we deemed insufficient for a robust variability analysis. Consequently, we dropped these objects, reducing our sample size to 315. For each of these white dwarf candidates, we quantify the scatter of the recalibrated g -band magnitudes with respect to their median value (and therefore the degree of variability) by calculating reduced χ^2 values (Fig. 2). We defined $\chi^2_{\text{red}} > 2.0$ as the threshold for selecting 26 variable white dwarf candidates. For each of these stars, we constructed multi-epoch light curves, calculated amplitudes, and retrieved SDSS images and spectra (where available; Table 1). The amplitude of the scatter in the data was calculated from the observed light curves using a Monte Carlo method. We randomly varied the magnitude of each data point using a Gaussian probability distribution whose width was set to the uncertainty in the Stripe82 magnitudes. For each re-sampling we calculate the amplitude as half of the difference between the brightest and faintest detection. The reported amplitudes are the averages of 1000 re-samplings. These values reflect the minimum expected amplitude of variability required to cause the observed scatter in the Stripe82 data.

All but one of our candidates (SDSSJ2157+0037, see Sect. 5.8) have an SDSS spectrum. Combining all available data (spectra, SDSS colours and images, χ^2_{red} and light curves) we then attempted to assess the nature of the observed variability.

3.1 Source contamination

If two sources in Stripe 82 happen to be spatially very close ($\lesssim 2''$), some of the measurements may suffer from poor deblending during variable seeing conditions, resulting in apparently variable multi-epoch photometry. Inspecting the SDSS images of the 26 variable white dwarf candidates, we found that SDSS J0342+0024 has a close, potentially contaminating neighbour (Fig. 3). We therefore decided to drop this star from our candidate list.

3.2 Errors in source extraction

While inspecting the light curves of our variable candidates, two objects stood out for having some extremely faint detections. SDSS J0106–0014 has two g -band magnitude measurements of 25.5 mag and 24.6 mag, while SDSS J2157–0044 has one g -band magnitude measurement of 24.7 mag. All these values are much fainter than the nominal g -band limit of SDSS, implying that the objects were most likely just at the edge of detection in those

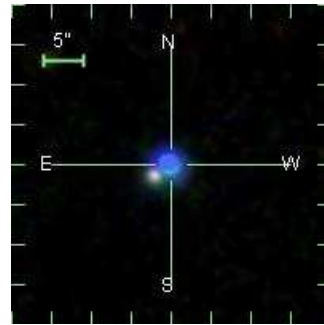


Figure 3. SDSS image of SDSS J0342+0024 showing possible contamination from nearby source.

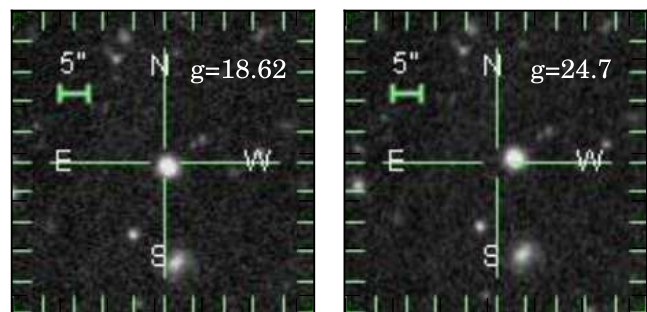


Figure 4. SDSS images of SDSSJ 2157–0044 centred at the position of one of the detections close to the median magnitude (*left panel*) and at the position of the faint detection (*right panel*).

nights. In both cases these magnitudes diverge dramatically from the median magnitude of the object ($g = 18.63$ for SDSS J2157–0044, $g = 18.15$ for SDSS J0106–0014), strongly contributing to the high reduced χ^2 values calculated for these objects. We decided to further verify the reliability of these measurements by checking the coordinates of the detections.

Figure 4 clearly shows that, in the case SDSS J2157–0044, the apparent dimming is due to an error in the position at which the source was extracted. However for SDSS J0106–0014 the coordinates of bright and faint detections are consistent, and we have to conclude that a genuine dimming was observed (see Sect. 5.3).

4 ZZ CETIS CANDIDATES

Since the ZZ Ceti instability strip is defined by a narrow range in temperature and surface gravity, a $u-g, g-r$ colour projection of the $T_{\text{eff}}/\log g$ strip can be used to select ZZ Ceti candidates (Mukadam et al. 2004; Greiss et al. 2014). By inspecting the colour-colour locus of known ZZ Ceti we selected from our variable candidate list ten stars most likely belonging to this class (Fig. 5, Table 2). However, as we discuss later, $u-g, g-r$ colours alone are not very efficient at discriminating between ZZ Ceti and non pulsating white dwarfs (see Sect. 4.3).

Table 1. Stripe82 photometric parameters of the 26 variable white dwarf candidates and the three non-variable white dwarfs (below the dashed line) selected as “control” objects. Median g magnitudes were calculated from all re-calibrated, reliable Stripe82 photometry. g scatter were calculated via a Monte Carlo method, and represent the minimum expected amplitudes of variability required to cause the observed scatter in the Stripe82 photometry. Colours were calculated using median magnitudes. Objects marked with † were later dropped as spurious candidates (see Sect. 3.1 and Sect. 3.2).

SDSS name	RA	Dec	median g mag	$u - g$	$g - r$	χ^2	g scatter (mag)
SDSS J0028–0012	00 28 03.34	–00 12 13.2	18.55	0.39	–0.26	3.3	0.10 ± 0.02
SDSS J0050–0001	00 50 13.52	–00 01 30.3	18.64	0.13	–0.31	3.4	0.10 ± 0.01
SDSS J0050–0023	00 50 47.61	–00 23 16.9	18.80	0.32	–0.089	2.7	0.12 ± 0.02
SDSS J0102–0033	01 02 07.32	–00 33 00.1	18.19	0.43	–0.11	2.7	0.09 ± 0.02
SDSS J0106–0014	01 06 22.99	–00 14 56.2	18.18	0.48	–0.20	4.3	3.71 ± 0.39
SDSS J0121–0028	01 21 02.30	–00 28 12.0	18.45	0.52	–0.15	8.7	0.11 ± 0.02
SDSS J0134–0109	01 34 40.94	–01 09 02.3	18.12	0.49	–0.03	2.6	0.09 ± 0.02
SDSS J0158–0000	01 58 01.11	–00 00 00.2	18.62	0.36	–0.22	5.1	0.16 ± 0.02
SDSS J0209+0050	02 09 27.68	+00 50 21.0	18.41	–0.03	–0.37	3.5	0.10 ± 0.02
SDSS J0247+0003	02 47 46.29	+00 03 31.6	16.26	0.24	–0.38	3.4	0.07 ± 0.01
SDSS J0318+0030	03 18 47.09	+00 30 29.5	17.86	0.42	–0.13	2.7	0.08 ± 0.02
SDSS J0321–0050	03 21 43.49	–00 50 25.6	18.89	0.27	–0.26	2.4	0.10 ± 0.02
SDSS J0326+0002	03 26 15.34	+00 02 21.6	18.44	0.08	–0.30	3.0	0.17 ± 0.02
SDSS J0326+0018	03 26 19.44	+00 18 17.5	17.41	0.39	–0.20	7.8	0.13 ± 0.01
SDSS J0342+0024†	03 42 29.96	+00 24 17.8	16.47	0.09	–0.18	5.7	0.29 ± 0.02
SDSS J0349–0059	03 49 17.40	–00 59 19.2	17.65	–0.39	–0.34	2.7	0.07 ± 0.01
SDSS J2109+0111	21 09 33.63	+01 11 10.6	18.96	0.12	–0.33	3.0	0.13 ± 0.02
SDSS J2156–0046	21 56 28.27	–00 46 17.2	18.38	0.55	–0.06	3.8	0.07 ± 0.01
SDSS J2157+0037	21 57 13.51	+00 37 14.8	17.41	0.51	–0.12	9.3	0.11 ± 0.01
SDSS J2157–0044†	21 57 11.87	–00 44 34.9	18.63	–0.35	–0.39	44.7	3.40 ± 0.25
SDSS J2218–0000	22 18 28.59	–00 00 12.2	18.09	0.15	–0.20	2.2	0.07 ± 0.01
SDSS J2220–0041	22 20 30.69	–00 41 07.3	17.48	0.43	0.11	2.8	0.07 ± 0.01
SDSS J2237–0101	22 37 26.85	–01 01 10.8	18.88	0.46	–0.11	4.8	0.12 ± 0.02
SDSS J2318–0114	23 18 41.50	–01 14 43.1	18.74	0.14	–0.32	2.2	0.15 ± 0.02
SDSS J2330+0100	23 30 40.50	+01 00 47.6	17.52	0.66	0.25	3.2	0.13 ± 0.02
SDSS J2333+0051	23 33 05.08	+00 51 55.6	18.55	–0.06	–0.32	5.0	0.16 ± 0.02

SDSS J0327+0012	03 27 27.52	+00 12 52.5	17.83	0.44	–0.17	0.8	0.04 ± 0.02
SDSS J2245–0040	22 45 18.53	–00 40 25.2	18.47	0.44	–0.17	0.6	0.04 ± 0.02
SDSS J2336–0051	23 36 47.00	–00 51 14.6	18.32	0.48	–0.20	0.7	0.05 ± 0.02

4.1 Follow up observations

We obtained high-speed photometry for six of our ten ZZ Ceti candidates and one V777 Her candidate (see Sect. 5.5) in order to confirm their pulsating nature. We used the optical imaging component of the IO (Infrared-Optical) suite of instruments (IO:O)¹ on the Liverpool Telescope (LT) on the island of La Palma. Each target was observed with 30s exposures for $\simeq 2$ hours. In order to verify the robustness of our multi-epoch variability selection we also observed three “control” white dwarfs which have colours compatible with those of ZZ Ceti, but for which we found no evidence of variability in multi-epoch data (i.e. $\chi_{\text{red}}^2 \leq 1.0$; Table 1).

4.2 Analysis and results: three new ZZ Ceti

We extracted sky-subtracted light curves from our LT observations and computed Fourier transforms (FT) for our six ZZ Ceti candidates, the three “control” DAs and one candidate V777 Her (see Sect. 5.5). We classified a candidate as a confirmed pulsating white dwarf if its FT shows a peak larger than 4 times the average amplitude of the entire FT and above a 3σ threshold (Greiss et al.

2014). Of the six ZZ Ceti candidates observed we detect pulsations for five of them. Two (SDSS J0102–0033 and SDSS J0318+0030) had already been identified as ZZ Ceti stars by Mukadam et al. (2004), while the remaining three (SDSS J0124–0109, SDSS J2157–0044 and SDSS J2237–0101²) are new discoveries (Fig. 6). We designate the remaining five objects (three “control” white dwarfs, one ZZ Ceti candidate and one V777 Her candidate) as “not observed to vary” (NOV) and estimate percentile non variability limits (Fig. 7). These results are reported in Table 2.

4.3 The ZZ Ceti instability strip

As mentioned in Section 4 we picked our ZZ Ceti candidates by selecting the Stripe82 variables which were closest to the $u - g, g - r$ projection of the ZZ Ceti instability strip. However, Fig. 8 reveals that many known NOVs are

² In the referee report, it was brought to our attention that SDSS J2237–0101 had been independently identified as a ZZ Ceti by Wolf et al. (2007, private communication) who selected SDSS J2237–0101 from a small sample of white dwarfs with SDSS spectroscopy which appeared in the preliminary Stripe82 variability catalogue of Ivezić et al. (2007).

¹ <http://telescope.livjm.ac.uk/TelInst/Inst/IOO/>

Table 2. Additional parameters of the 26 white dwarf candidates initially identified as variable sources and the three non-variable white dwarfs (below the dashed line) selected as “control” objects. Objects marked with † were later dropped as candidates. T_{eff} and $\log g$ are calculated using 1D atmospheric models. The initial class column shows the spectral classification we assigned to the object based on the available SDSS spectrum. “ZZ_{cand}” are ZZ Ceti candidates (Sect. 4). The “LT obs” column shows the results of our LT time series follow up. Object which were not observed to vary (in our LT follow up or by Mukadam et al. 2004) are flagged as “NOV” followed by the non variability limit set by the observations.

Object	T_{eff}^a [K]	$\log g^a$ [cgs]	initial class	LT obs.	remarks
SDSS J0028–0012	14,590±480	7.99±0.07	DA	–	–
SDSS J0050–0001	21,120±570	7.59±0.08	DA	–	–
SDSS J0050–0023	11,170±90	8.84±0.05	ZZ _{cand}	–	NOV0.6% ^b
SDSS J0102–0033	11,110±170	8.37±0.09	ZZ _{cand}	ZZ Ceti	ZZ Ceti ^b
SDSS J0106–0014	14,240±300	7.49±0.06	ZZ _{cand}	–	eclipsing binary ^c
SDSS J0121–0028	10,447±30 ^d	8.42±0.03 ^d	ZZ _{cand}	NOV1.4%	–
SDSS J0134–0109	10,490±80	8.04±0.07	ZZ _{cand}	ZZ Ceti	–
SDSS J0158–0000	13,020±440	8.29±0.09	ZZ _{cand}	–	–
SDSS J0209+0050	24,910±510	7.94±0.07	DA	–	–
SDSS J0247+0003	19,362±120	8.05±0.019	DA	–	–
SDSS J0318+0030	11,450±120	8.33±0.05	ZZ _{cand}	ZZ Ceti	ZZ Ceti ^b
SDSS J0321–0050	16,896±440 ^e	8.00±0.09 ^e	DAH	–	–
SDSS J0326+0002	21,710±320	7.93±0.05	DA	–	–
SDSS J0326+0018	12,570±90	8.17±0.03	ZZ _{cand}	–	NOV0.5% ^b
SDSS J0342+0024†	32,812±170 ^e	8.52±0.03 ^e	DAB	–	contam. (Sect.3.1)
SDSS J0349–0059	100,000±790 ^e	5.00±0.01 ^e	PG1159	–	known pulsator ^f
SDSS J2109+0111	20,530±340 ^e	7.81±0.05 ^e	DA	–	–
SDSS J2156–0046	10,940±150	8.20±0.09	ZZ _{cand}	ZZ Ceti	–
SDSS J2157+0037			no spec	–	see Sect. 5.8
SDSS J2157–0044†	60,420±5190	8.00±0.31	DA	–	pos. err (Sect. 3.2)
SDSS J2218–0000	12,239±440 ^e	9.73±0.24 ^e	MWD	–	–
SDSS J2220–0041	7730±40	7.98±0.07	DA	–	WD+BD ^g
SDSS J2237–0101	11,700±270	8.06±0.11	ZZ _{cand}	ZZ Ceti	–
SDSS J2318–0114	21,470±790	7.83±0.11	DA	–	–
SDSS J2330+0100	6660±60	8.23±0.13	DA	–	–
SDSS J2333+0051	22,857±890 ^e	8.09±0.07 ^e	V777 Her _{cand}	NOV2.1%	–

SDSS J0327+0012	16,800±220	8.59±0.03	DA	NOV1.2%	–
SDSS J2245–0040	13,260±300	8.12±0.07	DA	NOV4.2%	–
SDSS J2336–0051	12,860±330	7.80±0.09	DA	NOV3.0%	NOV0.5% ^b

^a Tremblay et al. (2011); ^b Mukadam et al. (2004); ^c Kleinman et al. (2004); ^d Kepler et al. (2015);

^e Kleinman et al. (2013); ^f Woudt et al. (2012); ^g Steele et al. (2009)

within the $u-g, g-r$ boundaries used; and vice versa, confirmed ZZ Ceti lie significantly outside the strip. Several studies have shown that a candidate selection purely based on colours yields a success rate of only 13 – 30 per cent (see Voss et al. 2006; Fontaine et al. 1982; Mukadam et al. 2004). Even though $u-g, g-r$ colours are good indicators of white dwarf temperature it appears that the narrow range of T_{eff} and $\log g$ that defines the ZZ Ceti instability strip does not unambiguously project to the observed colours. Furthermore, the $ugriz$ magnitudes of SDSS are not acquired simultaneously, but in the sequence $riuzg$, with observations in each filter separated by 71.72 s. As a result u and g band observations are performed roughly 143 seconds apart and g and r observation nearly 290 seconds apart. Cool pulsating white dwarfs can vary in brightness by up to 20 percent on such timescales, implying that the SDSS colours of these objects may be taken during different pulsation phases and are not, therefore, reliable indicators of temperature. Figure 9 clearly illustrates this effect, i.e. multi-epoch colours of confirmed ZZ Ceti exhibit much larger scatter in colour-colour space than those of confirmed NOV. Reddening too, though often considered to be a minor effect for relatively

nearby white dwarfs, may still contribute to the observed discrepancy between temperatures and colours.

If optical spectra are available, T_{eff} and $\log g$ can be measured from fitting the Balmer lines of DA white dwarfs. (Koester et al. 1979, Bergeron et al. 1995, Koester 2009, Tremblay et al. 2011). ZZ Ceti candidates can then be reliably selected on the basis of the atmospheric parameters (Bergeron 2001, Mukadam et al. 2004, Gianninas et al. 2011). Figure 8 illustrate that the majority of known ZZ Ceti (including the five confirmed as part of this work) lie within the boundaries of the empirical instability strip, with little contamination from NOV. Even though the spectroscopic method can achieve efficiency upwards of 80 per cent, the required large samples of spectroscopically confirmed DAs are observationally expensive.

In this pilot study we selected ZZ Ceti candidates without relying on spectroscopy and combining colour selection with the evidence of multi-epoch variability. Five out of the six candidates followed-up with high speed photometry, were confirmed to be ZZ Ceti (see Sect. 4.2), implying an efficiency $\simeq 83$ per cent. Even though limited to sparse data over only the 300 deg² of Stripe 82, we showed that, using

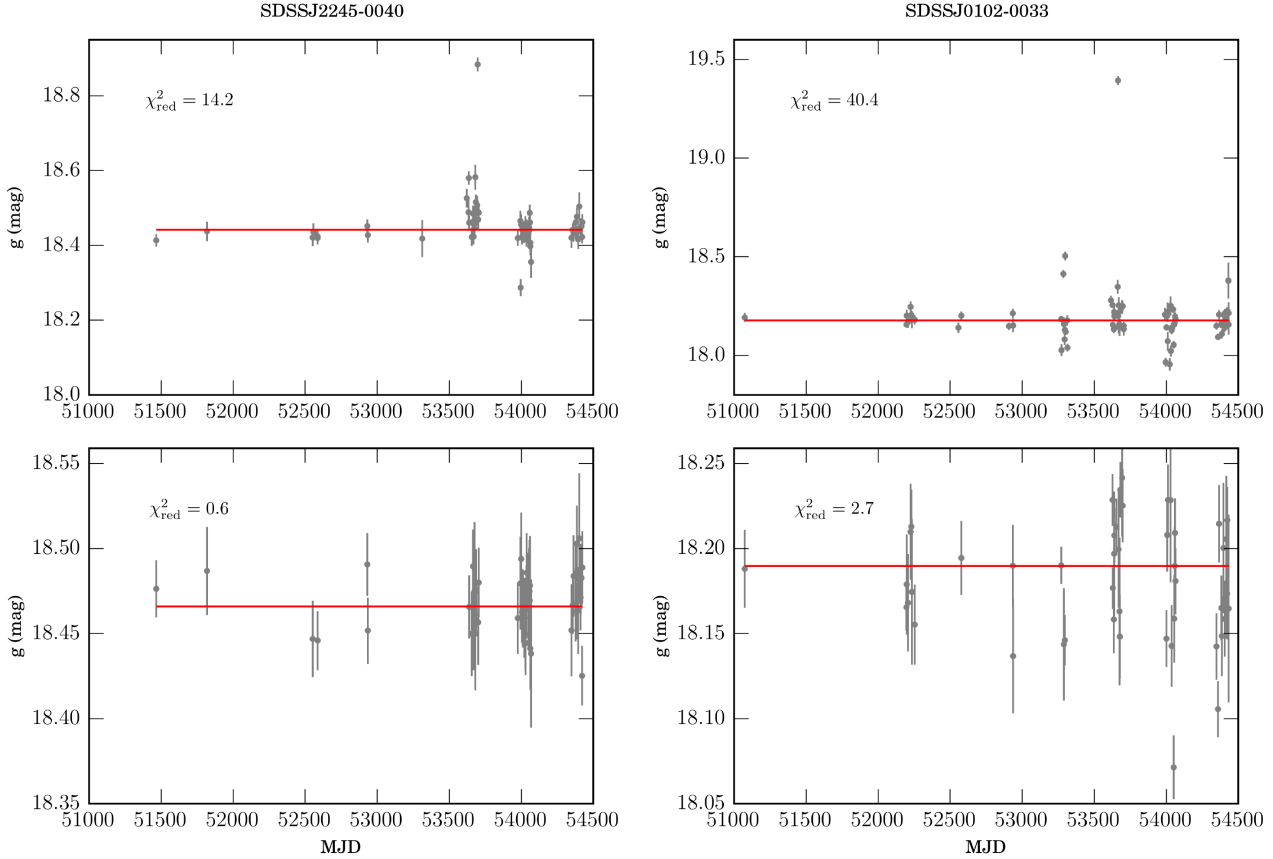


Figure 2. Multi-epoch light curves of the “control” white dwarf SDSS J2245–0044 (*left*) and the confirmed ZZ Ceti SDSS J0102–0033 (*right*). *Top panels:* all available Stripe82 data with the default calibration. *Bottom panels:* Multi-epoch light curves of the same stars after re-calibrating the photometry and discarding unreliable nights. The red line indicates the median magnitude values.

multi-epoch data, it is possible to achieve an efficiency similar to that of the spectroscopic selection method. However it is important to keep in mind that our statistics is limited to only the six ZZ Ceti candidates we followed up with LT observations. Our selection method is biased in favour of cool, high-amplitude ZZ Ceti (see Sect. 4.4) and our three newly identified ZZ Ceti are among the coolest ever discovered. With their identification we empirically constrain the red edge of the instability strip. Applying this selection to other current and future time domain surveys (e.g. PanSTARRS, LSST) will provide very large samples of high-confidence ZZ Ceti candidates, paving the way for global ensemble asteroseismology of white dwarfs.

4.4 Pulsation properties of the ZZ Ceti variables

We list the dominant periods found for the five confirmed ZZ Ceti in Table 3. All five ZZ Ceti undergo large amplitude pulsation with periods longer than 600s, which are normally associated with cool ZZ Ceti ($T_{\text{eff}} \simeq 11,000$ K). Fig. 8 clearly shows that all our confirmed ZZ Ceti are indeed cool pulsators, with three of them lying on the red edge of the instability strip. This selection effect is caused by the fact that pulsation amplitude increases with decreasing T_{eff} . Since variability with amplitudes $\lesssim 0.03$ mag would not be

Table 3. Pulsation properties of the five confirmed ZZ Ceti. Three new ZZ Ceti discovered as part of this work are marked with *.

name	period (s)	amplitude (mma)
SDSS J0102–0033	796.1 ± 3.7	75.1 ± 6.5
SDSS J0134–0109*	1212 ± 13	45.4 ± 5.9
SDSS J0318+0030	969 ± 11	21.8 ± 3.5
	746.4 ± 6.7	21.1 ± 3.5
SDSS J2156–0046*	1234 ± 15	31.4 ± 4.1
	1478 ± 21	27.0 ± 3.5
SDSS J2237–0101*	774.4 ± 4.6	80.1 ± 8.5
	392.3 ± 2.2	44.7 ± 8.3

detectable in the Stripe82 data, we are biased to preferentially select cool, large-amplitude ZZ Ceti.

Mukadam et al. (2004) report periods for SDSS J0102–0033 (926.1 s, 830.3 s) and SDSS J0318+0030 (826.4 s, 587.1 s, 536.1 s) compatible with cool ZZ Ceti, but significantly different from the period reported here. Such changes in pulsation periods over long time scales are not uncommon, as cool ZZ Ceti are known to undergo amplitude and frequency variations (e.g. G29–38, McGraw & Robinson 1975; Kleinman et al. 1998; GD 1212, Hermes et al. 2014).

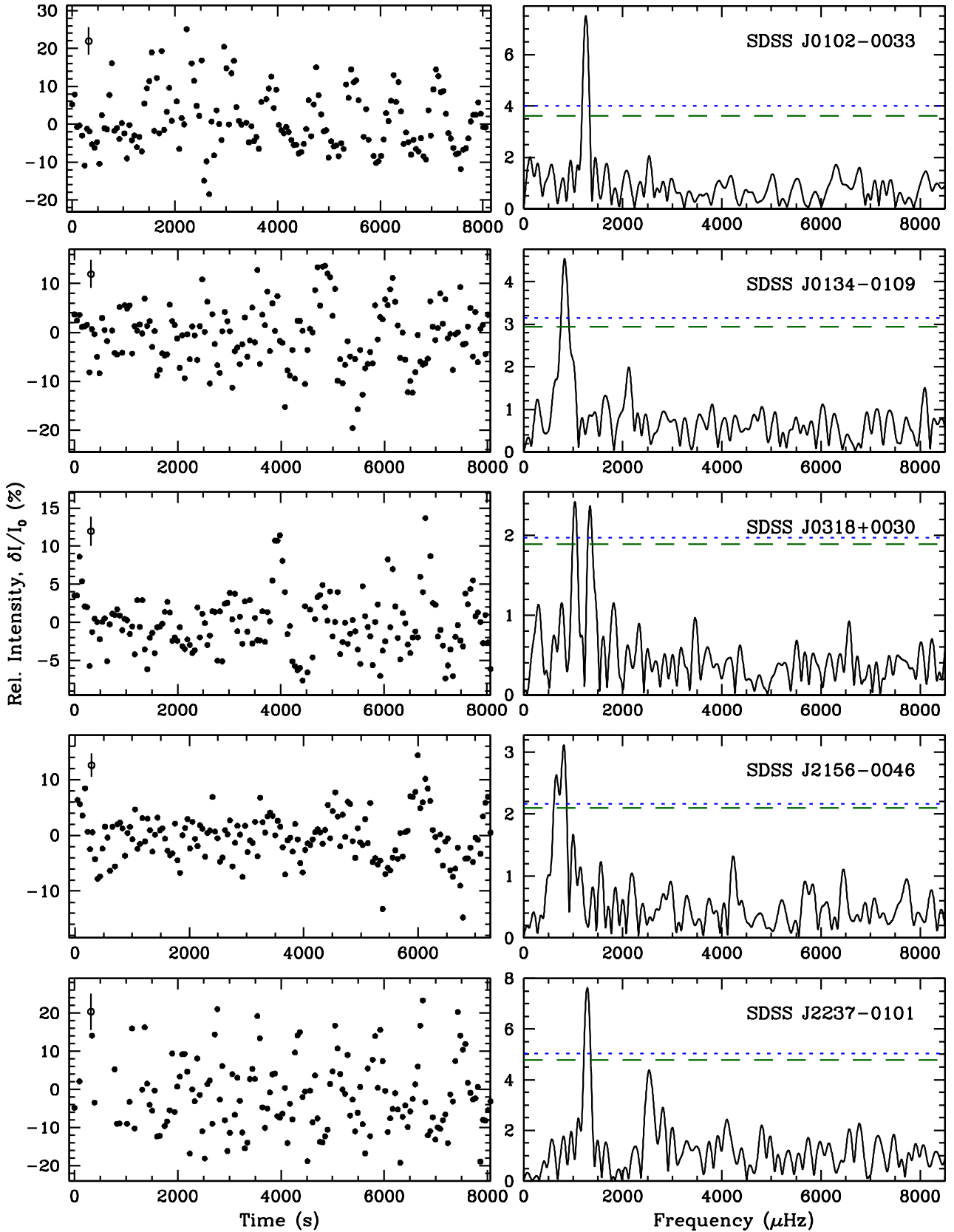


Figure 6. LT lightcurves (left) and corresponding Fourier transforms (right) for the five ZZ Ceti candidates which were confirmed as pulsating white dwarfs. Typical photometric uncertainties are indicated in the top left of each panel. The green dashed line marks 4 times the average amplitude of the entire Fourier transform; the blue dotted line marks the 3-sigma significance threshold, as determined by 10,000 bootstrap shuffles of the light curve (for more details see Greiss et al. 2014). SDSS J0134-0109, SDSS J2237-0101 and SDSS J2156-0046 are new high-amplitude ZZ Ceti discoveries.

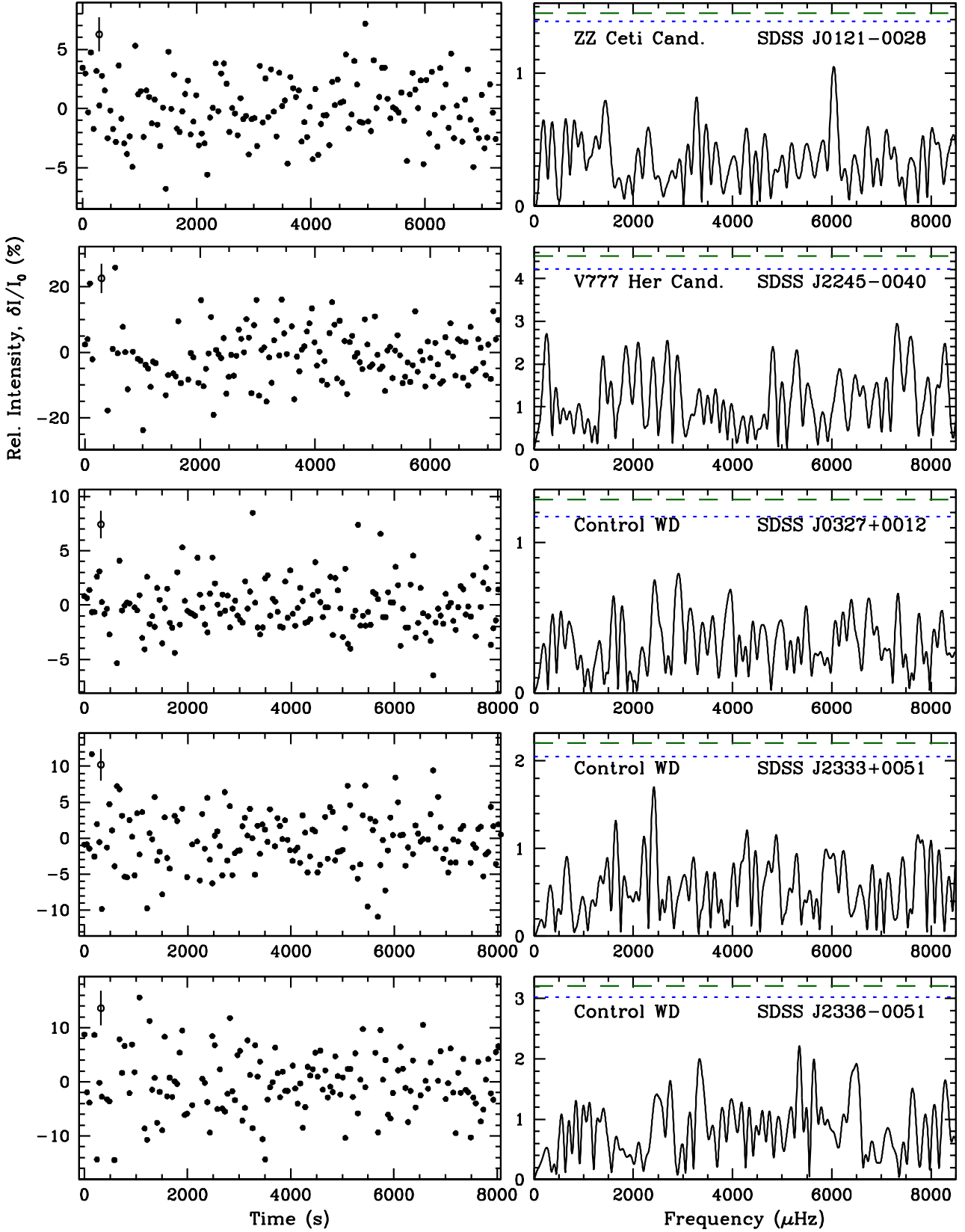


Figure 7. As Figure 6 for the five objects for which we detected no variability in our LT observations. SDSS J0327+0012, SDSS J2245-0040 and SDSS J2336-0051 have colours compatible with those of ZZ Ceti, but show no evidence of variability in their Stripe 82 data (“control” white dwarfs). Our observations do not completely rule out the presence of pulsations, as all objects may vary at smaller amplitudes; the maximum pulsation amplitude of known ZZ Ceti has a median of 1.5 per cent in the SDSS g band.

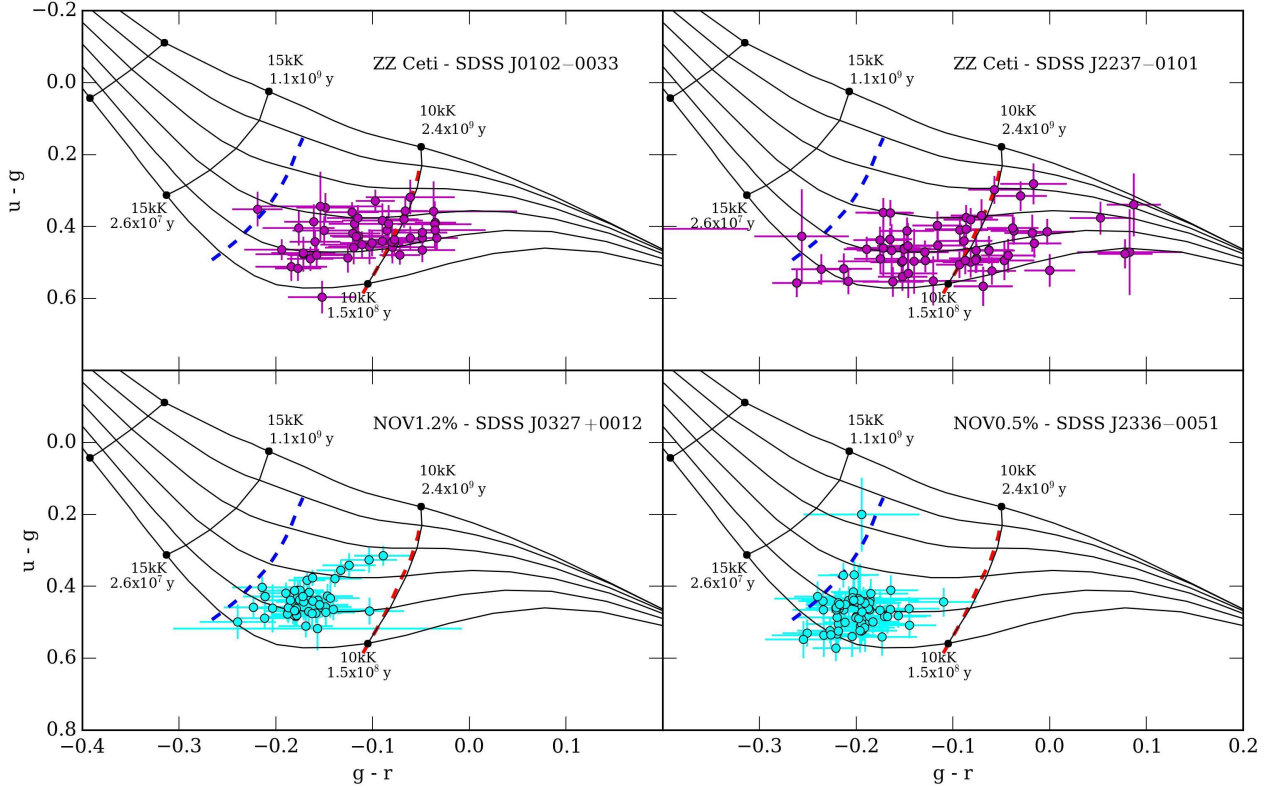


Figure 9. Colour-colour distribution of all reliable recalibrated Stripe82 epochs of two confirmed ZZ Ceti (SDSS J0102–0033, SDSS J2237–0101, *top panels*, magenta points) and two confirmed NOV, “control” white dwarfs (SDSS J2245–0040 and SDSS J2336–0051, *bottom panels*, cyan points). The empirical blue and red edge of the ZZ Ceti instability strip are shown as a blue and a red dashed line, respectively.

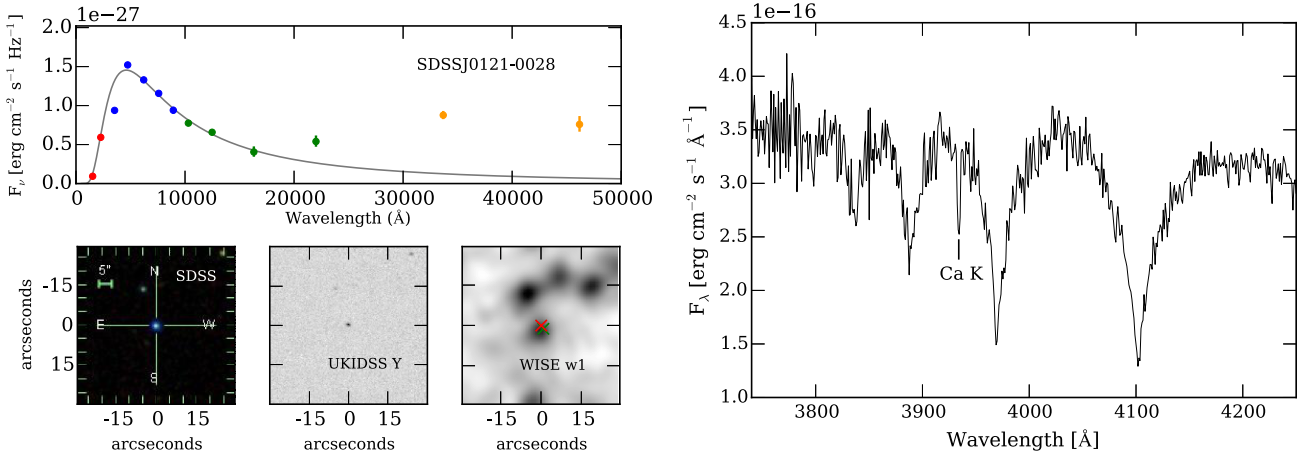


Figure 10. *Left panel:* Spectral energy distribution of SDSS J0121–0028. Galex *fuv, nuv* fluxes are plotted in red, SDSS Stripe82 recalibrated median *ugriz* fluxes in blue, UKIDSS *YJHK* fluxes in green and WISE *w1, w2* fluxes in yellow. The grey solid line shows a blackbody model of the white dwarf fitted to the *g* and *r* fluxes. *Right panel:* SDSS spectrum of SDSS J0121–0028 showing the presence of Ca K absorption line.

5 NOTES ON SINGLE OBJECTS

5.1 SDSS J0121–0028

Based on its $u - g; g - r$ colours, SDSS J0121–0028 was selected as a ZZ Ceti candidate, but in our two hours high-

speed photometric follow-up we did not observe any pulsation to a limit of 1.39 per cent. The amplitude of the variation calculated from the Stripe82 data (8–10 per cent, Table 1) is above this non-variability threshold, possibly implying that our LT observations were taken during a period of destructive interference of the pulsation modes

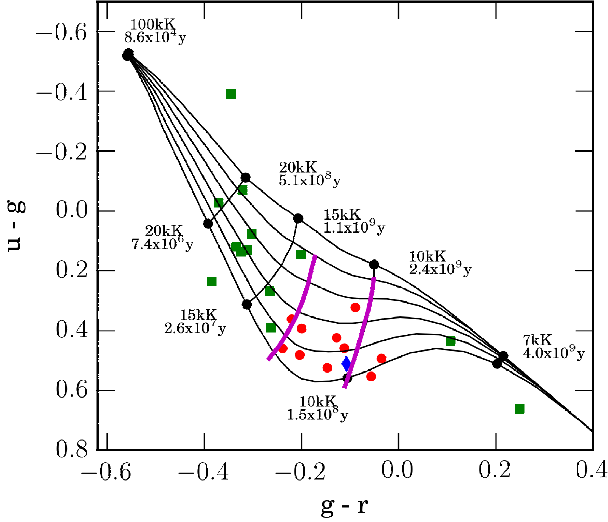


Figure 5. $u - g, g - r$ colour-colour distribution of our sample of Stripe82 variable white dwarfs candidates: ZZ Ceti candidates as red circles, one candidate with no SDSS spectroscopy (see Sect. 5.8) as the blue diamond and remaining candidates as green squares. The magenta lines show the empirical boundary of the ZZ Ceti instability strip from Gianninas et al. (2014). White dwarf cooling tracks from Holberg & Bergeron (2006) are shown in the overlay. The colours of our variable candidates have been computed using the median magnitude values.

(e.g. Castanheira et al. 2006). Nonetheless, Fig. 8 shows that SDSS J0121–0028 lies outside the ZZ Ceti instability strip, red-ward of the the red edge. If SDSS J0121–0028 is indeed a ZZ Ceti it would be a rare, though not unprecedented, outlier (e.g. WD J0940+0050, Castanheira et al. 2013). Another possibility is that SDSS J0121–0028 undergoes some other type of magnitude variation on timescales longer than 2 hours.

To further investigate the nature of SDSS J0121–0028, we retrieved all available ultraviolet and mid-infrared photometry of SDSS J0121–0028. The spectral energy distribution of SDSS J0121–0028 (Fig. 10) shows a marked infrared excess which is not consistent with a single, isolated white dwarf. The presence of a close, low-mass companion could explain the observed infrared excess and companions may also cause some degree of optical variability in white dwarfs (Littlefair et al. 2014; Casewell et al. 2015; Maoz et al. 2015).

However the infrared excess in SDSS J0121–0028 becomes apparent only in the UKIDSS K band, rising towards longer wavelengths. A blackbody fit to this infrared emission, adopting the photometric distance of the white dwarf, suggests a $T_{\text{eff}} \simeq 1100$ K and radius $\simeq 2.1$ Jupiter radii (R_J), i.e. more than twice the radius of a typical brown dwarf ($0.83 R_J$, Sorahana et al. 2013). It therefore seems unlikely that the infrared excess is caused by a brown dwarf companion. An alternative origin of the infrared excess could be a circumstellar debris discs resulting from tidal disruption of rocky planetesimals (Graham et al. 1990; Jura 2003), and $\simeq 1 - 3.5$ per cent of all white dwarfs exhibit infrared excesses consistent with the presence of such discs (Farihi et al. 2009; Girven et al. 2011; Rocchetto et al. 2015). In all cases the presence of these discs is accompanied with metal pol-

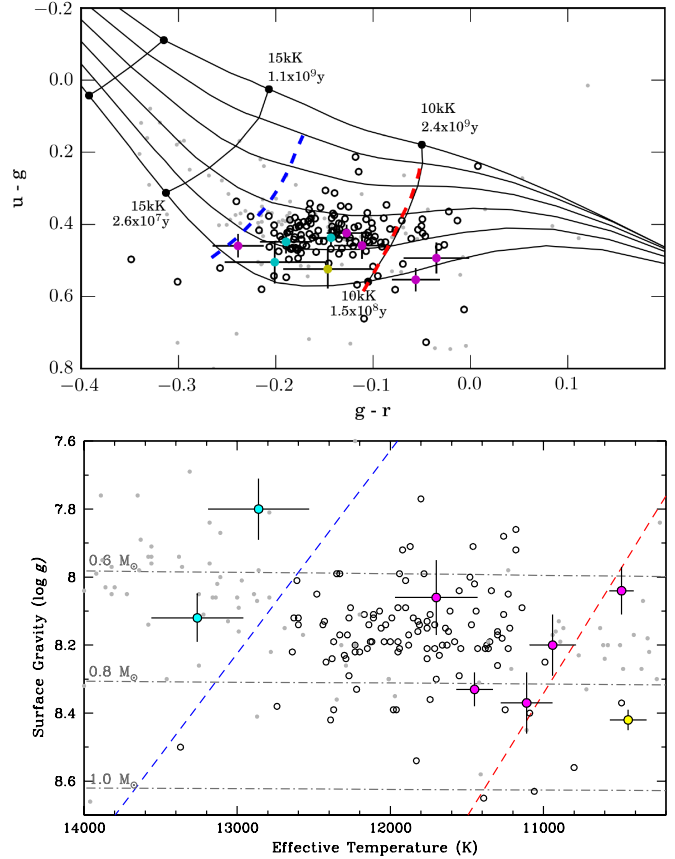


Figure 8. Colour distribution (*top panel*), and $T_{\text{eff}} - \log g$ distribution (*bottom panel*) of known ZZ Cetis (empty circles) and NOVs (grey dots). $\log g$ and T_{eff} values were taken from Tremblay et al. (2011) and Gianninas et al. (2011) and are calculated using 1D atmospheric models. The empirical blue and red edge of the ZZ Ceti instability strip are shown as a blue and a red dashed line, respectively. We include our confirmed ZZ Cetis as magenta dots and our “control” white dwarf confirmed as NOVs as cyan dots (Table 2) and the ZZ Ceti candidate SDSS J0121–0028 (Sect. 5.1) as a yellow dot. The “control” white dwarf SDSS J0327+0012 is outside the range of the plot in the bottom diagram.

lution of the white dwarf atmosphere. Close inspection of the SDSS spectrum of SDSS J0121–0028 reveals a strong calcium absorption line at 3933.7Å, identifying it as a metal polluted DAZ white dwarf (Fig. 10). The presence of metals in the photosphere of SDSS J0121–0028 strongly supports the hypothesis that the observed infrared excess is due to a debris disc. There is growing evidence of variability in some white dwarf debris discs, including changes in the optical line profiles (Gänsicke et al. 2008; Wilson et al. 2015) and line fluxes (Wilson et al. 2014) from gaseous discs, as well as changes in the infrared flux from the dust (Xu & Jura 2014). However, to date, optical variability in white dwarfs with debris discs has only been observed at amplitudes much lower than what we measured for SDSS J0121–0028. The data at hand does not allow to unambiguously determine the nature of the variability of SDSS J0121–0028 and we recommend further observations of this object.

5.2 SDSS J0050–0023 and SDSS J0326+0018

Two of our ZZ Ceti candidates had already been observed by Mukadam et al. (2004) and found not to vary: SDSS J0050–0023 and SDSS J0326+0018. We did not acquire more observations, but the NOV limits calculated by Mukadam et al. (2004) are considerably smaller than the amplitudes of the variability detected in the Stripe82 data (> 0.1 mag; Table 1). Again this implies that these white dwarfs may vary on longer timescales.

SDSS J0050–0023 is known massive white dwarf with spectroscopic mass above a $1M_{\odot}$ (Castanheira et al. 2010). At the temperatures around the ZZ Ceti instability strip, stars with such mass are expected to be up to 90 per cent crystallized (Kanaan et al. 2005). Crystallization has significant effect on the pulsation properties of a white dwarfs since pulsations cannot propagate into the crystallized region (Montgomery & Winget 1999). Pulsating massive white dwarfs can therefore experience dramatic changes in their pulsation amplitudes (e.g. BPM37093, McGraw 1976; Kanaan et al. 1998).

SDSS J0050–0023 was classified as NOV6 by Mukadam et al. (2004) and NOV3.7 by Castanheira et al. (2010), however Castanheira et al. (2010) also report possible, lower-amplitude pulsations with a period of 584s. The multi-epoch variability observed in Stripe82 seems to validate the hypothesis that SDSS J0050–0023 is a massive pulsator with highly variable pulsation amplitudes. It is possible that all high-cadence monitoring to date was carried out during a phases of pulsation dampening and consequently failed to identify pulsations. We encourage further, long-term monitoring of SDSS J0050–0023 to determine if the star is truly variable.

5.3 SDSS J0106–0014: an eclipsing binary

In Sect. 3.2 we mentioned that the Stripe82 data of SDSS J0106–0014 contains two extremely faint, but reliable detections. Literature research revealed that SDSS J0106–0014 is a known eclipsing binary system (Kleinman et al. 2004). Previous observation of this objects reported a period of 0.085 days with a mid-eclipse time at MJD 55059.051 (Parsons et al. 2015). This ephemeris confirms that the dim detection of SDSS at MJD 53697.271 and 52522.362 indeed correspond to observations taken in eclipse.

5.4 Magnetic White Dwarfs

At least 4 per cent of all known white dwarfs have magnetic fields in the range 2–1000 MG (Schmidt & Smith 1995; Liebert et al. 2003; Kepler et al. 2013; Kleinman et al. 2013). The mechanism that leads to the formation of strong magnetic fields in white dwarfs is still subject of debate, with several plausible mechanics being proposed: fossil fields conserved in the evolution of peculiar Ap and Bp stars (Angel & Landstreet 1970; Angel et al. 1981; Wickramasinghe & Ferrario 2000); fields generated by a magnetic dynamo during a phase of binary evolution (Tout et al. 2008; Nordhaus et al. 2011); and fields generated in differentially rotating white dwarfs with convective envelopes (Markiel et al. 1994).

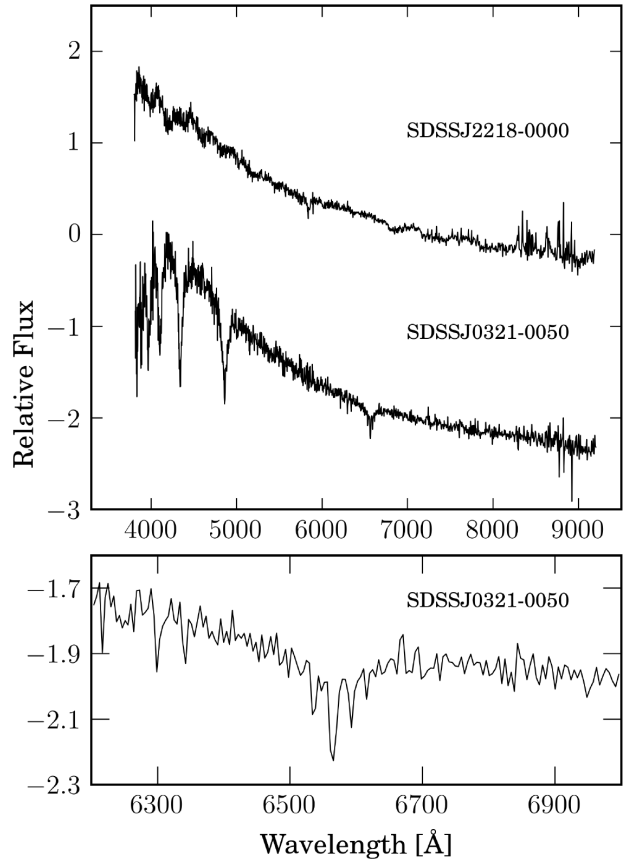


Figure 11. SDSS spectra of SDSS J2218–0000 and SDSS J0321–0050. In SDSS J2218–0000 the high magnetic field (≈ 225 MG) splits and significantly blurs the Balmer lines beyond recognition. In the case of SDSS J0321–0050 the presence of a weak field (≈ 1.4 MG) is revealed by Zeeman splitting of the $H\alpha$ absorption line (*bottom panel*).

Some magnetic white dwarfs also exhibit photometric modulation, most likely caused by stellar rotation combined with localized magnetic dichroism (Brinkworth et al. 2013) or, in the case on convective white dwarfs (i.e. $T_{\text{eff}} \lesssim 13,000$ K for DAs), the presence of star-spots (Lawrie et al. 2013). The rotation period of magnetic white dwarfs can potentially discriminate between different evolutionary scenarios and provide some insight on the origin of the field.

Inspecting the SDSS spectra available for our 26 Stripe 82 variable candidates, we identify two magnetic white dwarfs: SDSS J2218–0000 and SDSS J0321–0050. The Zeeman splitting of $H\alpha$ in SDSS J0321–0050 is very weak (Fig. 11). In fact, this star was previously classified as a non-magnetic DA (Eisenstein et al. 2006; Kleinman et al. 2013; Gentile Fusillo et al. 2015). Following Reid et al. (2001), we estimate the average surface magnetic field strength, B_s , according to the equation:

$$B_s/\text{MG} = \frac{\Delta(1/\lambda)}{46.686}, \quad (1)$$

where $\Delta(1/\lambda)$ is the inverse wavelength separation in cm^{-1} between the components of a Zeeman triplet (Reid et al. 2001); and find $B_s = 1.36 \pm 0.04$ MG. In contrast, SDSS J2218–0000 was already identified as a magnetic

white dwarf and has a field sufficiently strong to smear out most of the Balmer lines ($B_s \simeq 225$ MG, Schmidt et al. 2003; Külebi et al. 2009)

5.5 The V777 Her candidate SDSS J2333+0051

Among our variable candidates we identified one DB white dwarf (SDSS J2333+0051). With only $\simeq 20$ V777 Her stars known to date, a robust definition of a DB white dwarfs instability strip, both empirical and theoretical, is still an ongoing challenge (Kilkenny et al. 2009, Nitta et al. 2009). Current evidence suggests that canonical $0.6 M_\odot$ DB white dwarfs undergo pulsation as they cool between roughly 29,000 K and 21,000 K (Nitta et al. 2009). SDSS J2333+0051 has $T_{\text{eff}} = 22,857$ K and $\log g = 8.09$ (Kleinman et al. 2013; Table 2) and is therefore a likely V777 Her candidate. As for our ZZ Ceti candidates, we obtained high-speed photometry of SDSS J2333+0051 and carried out the required Fourier space analysis (Sect. 4.1). We did not detect pulsations in SDSS J2333+0051 to a limit of 2.1 per cent. Based only on this result we cannot conclusively exclude that SDSS J2333+0051 is a V777 Her, as it may have lower amplitude pulsations. However the multi-epoch Stripe82 variability observed for SDSS J2333+0051 has a larger amplitude (0.16 ± 0.02 mag, Table 1) than the limit obtained by our LT observations. It is therefore possible that this white dwarf probably undergoes larger amplitude variations on longer timescales and we therefore encourage further observations of this star.

5.6 The PG1159 star SDSS J0349–0059

By inspecting the available SDSS spectra we identified one of our variable candidate, SDSS J0349–0059, as a PG1159 star (Table 2). SDSS J0349–0059 is a well studied object and a known pulsator (Woudt et al. 2012). Being able to independently recover a pulsating PG1159 star further proves the reliability of our selection method.

5.7 SDSS J2220–0041, a white dwarf plus brown dwarf binary

One of our variable candidates, SDSS J2220–0041, is a known white dwarf plus brown dwarf binary (PHL 5038, Steele et al. 2009). The presence of a low mass companion can, in some cases, cause some optical variability. Such variability is normally the result of irradiation of a tidally locked brown dwarf or ellipsoidal modulations (Littlefair et al. 2014; Casewell et al. 2015; Maoz et al. 2015). Both these mechanisms require the stars in the binary to be very close, but SDSS J2220–0041 is instead a wide binary system. The two stars in the system are spatially resolved at an angular separation of $0.94''$; corresponding to an orbital separation of $\simeq 55$ AU (Steele et al. 2009). The Stripe82 data alone does not allow to identify the nature of the variability or to speculate on a possible connection with the presence of the brown dwarf companion.

5.8 The white dwarf candidate SDSS J2157+0037

Stripe 82 has been the subject of many diverse studies and, consequently, it is one of the areas of the SDSS footprint with highest spectroscopic completeness. Indeed, of the 400 white dwarf candidates in our initial sample only 69 have no have a SDSS spectrum, and of the final 26 variable candidates found by our selection algorithm only one object, SDSS J2157+0037, lacks SDSS spectroscopy. We can therefore only speculate about the nature of the observed variability. Its $u - g(0.51)$ and $g - r(-0.11)$ colours are compatible with those of ZZ Ceti stars (Fig. 5). Furthermore, the amplitude measured from its Stripe82 lightcurve is similar to those of the confirmed ZZ Ceti in our sample. Again we encourage further observation of this object.

6 CONCLUSIONS

We have developed a method to select variable white dwarfs in large-area time domain surveys. Starting from a sample of white dwarf candidates, our method allows to correct and select reliable photometry using observations of neighbouring non-variable objects. Using this recalibrated photometry we then selected variable white dwarf candidates. We test our selection algorithm with a pilot search for pulsating white dwarfs in the SDSS Stripe82.

From a sample of 400 white dwarf candidates taken from Gentile Fusillo et al. (2015), we identified 24 variable candidates. From these 24 objects we further selected ZZ Ceti candidates using $u - g, g - r$ colours and acquired high-speed photometric follow up of six targets. We confirm five of our candidates as cool ZZ Ceti, three of which are new discoveries. Selection purely based on colour typically yields a success rate of only 13–30. We show that non simultaneous multi-band photometry is one of the causes of this low efficiency as it leads to unreliable colours for cool pulsating white dwarfs. However, we show that colour selection, combined with evidence of multi-epoch variability, significantly improves the quality of the ZZ Ceti candidates, without recourse to spectroscopy, achieving an efficiency of more than 80 per cent.

Among our candidates we also recover one known pulsating PG1159 star and one known eclipsing binary. We speculate on the most likely cause for the observed variability of the remaining candidates. Even though we recommend further observations to confirm beyond any doubt the variable nature of all our candidates, this pilot study already reveals the ability of our method to efficiently identify different types of variable white dwarf from eclipsing binaries to large amplitude cool pulsating white dwarfs.

SDSS Stripe82 proved a useful resource for testing our selection method, but covers only 300 deg^2 of the sky, with sparse observations taken under variable observing conditions. Upcoming time-domain surveys will cover much larger areas of the sky with more continuous cadence (eg. PTF, Law et al. 2009; Pan-STARRS, Morgan et al. 2014; Gaia, Walton 2014; LSST, Ivezić et al. 2011). The application of our selection method to these surveys will lead to identification of variable white dwarfs on industrial scale and provide very large samples of high-confidence ZZ Ceti candidates. In this pilot study we were aided by the high spectroscopic com-

pleteness of Stripe 82, but given the large area coverage of future time-domain surveys, such intense spectroscopic follow-up may not always be available. The photometric selection method presented in Gentile Fusillo et al. (2015) will perfectly complement future searches for variable white dwarfs providing large samples of high-confidence white dwarf candidates.

ACKNOWLEDGEMENTS

NPGF acknowledges the support of Science and Technology Facilities Council (STFC) studentships. The research leading to these results has received funding from the European Research Council under the European Unions Seventh Framework Programme (FP/2007-2013) / ERC Grant Agreement n. 320964 (WDTracer). We thank the referee for the constructive review. Funding for SDSS-III has been provided by the Alfred P. Sloan Foundation, the Participating Institutions, the National Science Foundation, and the U.S. Department of Energy Office of Science. The SDSS-III web site is <http://www.sdss3.org/>.

REFERENCES

- Abazajian, K. N., et al., 2009, *ApJS*, 182, 543
- Alam, S., et al., 2015, *ApJ*, 219, 12
- Althaus, L. G., Córscico, A. H., Isern, J., García-Berro, E., 2010, *A&A Rev.*, 18, 471
- Angel, J. R. P., Landstreet, J. D., 1970, *ApJ Lett.*, 160, L147
- Angel, J. R. P., Borra, E. F., Landstreet, J. D., 1981, *ApJS*, 45, 457
- Barstow, M. A., Jordan, S., O’Donoghue, D., Burleigh, M. R., Napiwotzki, R., Harrop-Allin, M. K., 1995, *MNRAS*, 277, 971
- Becker, A. C., Bochanski, J. J., Hawley, S. L., Ivezić, Ž., Kowalski, A. F., Sesar, B., West, A. A., 2011, *ApJ*, 731, 17
- Bergeron, P., 2001, *ApJ*, 558, 369
- Bergeron, P., Wesemael, F., Fontaine, G., 1992, *ApJ*, 387, 288
- Bergeron, P., Wesemael, F., Lamontagne, R., Fontaine, G., Saffer, R. A., Allard, N. F., 1995, *ApJ*, 449, 258
- Bergeron, P., Fontaine, G., Billères, M., Boudreault, S., Green, E. M., 2004, *ApJ*, 600, 404
- Bramich, D. M., et al., 2008, *MNRAS*, 386, 887
- Brinkworth, C. S., Burleigh, M. R., Wynn, G. A., Marsh, T. R., 2004, *MNRAS*, 348, L33
- Brinkworth, C. S., Burleigh, M. R., Lawrie, K., Marsh, T. R., Knigge, C., 2013, *ApJ*, 773, 47
- Casewell, S. L., et al., 2015, *MNRAS*, 447, 3218
- Castanheira, B. G., Kepler, S. O., Kleinman, S. J., Nitta, A., Fraga, L., 2010, *MNRAS*, 405, 2561
- Castanheira, B. G., Kepler, S. O., Kleinman, S. J., Nitta, A., Fraga, L., 2013, *MNRAS*, 430, 50
- Castanheira, B. G., et al., 2006, *A&A*, 450, 227
- Charpinet, S., Fontaine, G., Brassard, P., 2009, *Nat*, 461, 501
- Clemens, J. C., 1993, Ph.D. thesis, Univ. Texas at Austin
- Drake, A., 2014, in Wozniak, P. R., Graham, M. J., Mahabal, A. A., Seaman, R., eds., *The Third Hot-wiring the Transient Universe Workshop*, p. 37
- Eisenstein, D. J., et al., 2006, *ApJS*, 167, 40
- Farihi, J., Jura, M., Zuckerman, B., 2009, *ApJ*, 694, 805
- Fontaine, G., Brassard, P., 2008, *PASP*, 120, 1043
- Fontaine, G., Lacombe, P., McGraw, J. T., Dearborn, D. S. P., Gustafson, J., 1982, *ApJ*, 258, 651
- Fontaine, G., Bergeron, P., Lacombe, P., Lamontagne, R., Talon, A., 1985, *AJ*, 90, 1094
- Fontaine, G., Bergeron, P., Billères, M., Charpinet, S., 2003, *ApJ*, 591, 1184
- Fontaine, G., Brassard, P., Dufour, P., 2008, *A&A*, 483, L1
- Frieman, J. A., et al., 2008, *AJ*, 135, 338
- Gänsicke, B. T., Koester, D., Marsh, T. R., Rebassa-Mansergas, A., Southworth, J., 2008, *MNRAS*, 391, L103
- Gentile Fusillo, N. P., Gänsicke, B. T., Greiss, S., 2015, *MNRAS*, 448, 2260
- Gianninas, A., Bergeron, P., Ruiz, M. T., 2011, *ApJ*, 743, 138
- Gianninas, A., Dufour, P., Kilic, M., Brown, W. R., Bergeron, P., Hermes, J. J., 2014, *ApJ*, 794, 35
- Girven, J., Gänsicke, B. T., Steeghs, D., Koester, D., 2011, *MNRAS*, 417, 1210
- Graham, J. R., Matthews, K., Neugebauer, G., Soifer, B. T., 1990, *ApJ*, 357, 216
- Green, R. F., Richstone, D. O., Schmidt, M., 1978, *ApJ*, 224, 892
- Greiss, S., Gänsicke, B. T., Hermes, J. J., Steeghs, D., Koester, D., Ramsay, G., Barclay, T., Townsley, D. M., 2014, *MNRAS*, 438, 3086
- Hermes, J. J., et al., 2013, *MNRAS*, 436, 3573
- Hermes, J. J., et al., 2014, *ApJ*, 789, 85
- Holberg, J. B., Bergeron, P., 2006, *AJ*, 132, 1221
- Holberg, J. B., Howell, S. B., 2011, *AJ*, 142, 62
- Ivezic, Z., Strauss, M. A., Tyson, J. A., Axelrod, T., Bloom, J. S., LSST Collaboration, 2011, in *American Astronomical Society Meeting Abstracts #217*, vol. 43 of *Bulletin of the American Astronomical Society*, p. 252.01
- Ivezić, Ž., et al., 2007, *AJ*, 134, 973
- Jura, M., 2003, *ApJ Lett.*, 584, L91
- Kanaan, A., Kepler, S. O., Giovannini, O., Winget, D. E., Montgomery, M., Nitta, A., 1998, *Baltic Astronomy*, 7, 183
- Kanaan, A., et al., 2005, *A&A*, 432, 219
- Kepler, S. O., et al., 2013, *MNRAS*, 429, 2934
- Kepler, S. O., et al., 2015, *MNRAS*, 446, 4078
- Kilkenny, D., O’Donoghue, D., Crause, L. A., Hambly, N., MacGillivray, H., 2009, *MNRAS*, 397, 453
- Kleinman, S. J., et al., 1998, *ApJ*, 495, 424
- Kleinman, S. J., et al., 2004, *ApJ*, 607, 426
- Kleinman, S. J., et al., 2013, *ApJS*, 204, 5
- Koester, D., 2009, *A&A*, 498, 517
- Koester, D., Schulz, H., Weidemann, V., 1979, *A&A*, 76, 262
- Külebi, B., Jordan, S., Euchner, F., Gänsicke, B. T., Hirsch, H., 2009, *A&A*, 506, 1341
- Landolt, A. U., 1968, *ApJ*, 153, 151
- Lasker, B. M., Hesser, J. E., 1971, *ApJ*, 163, L89
- Law, N. M., et al., 2009, *PASP*, 121, 1395
- Law, N. M., et al., 2015, *PASP*, 127, 234

- Lawrie, K. A., Burleigh, M. R., Dufour, P., Hodgkin, S. T., 2013, *MNRAS*, 433, 1599
- Liebert, J., Bergeron, P., Holberg, J. B., 2003, *AJ*, 125, 348
- Littlefair, S. P., et al., 2014, *MNRAS*, 445, 2106
- Maoz, D., Mazeh, T., McQuillan, A., 2015, *MNRAS*, 447, 1749
- Markiel, J. A., Thomas, J. H., van Horn, H. M., 1994, *ApJ*, 430, 834
- McGraw, J. T., 1976, *ApJ*, 210, L35
- McGraw, J. T., Robinson, E. L., 1975, *ApJ*, 200, L89
- McGraw, J. T., Liebert, J., Starrfield, S. G., Green, R., 1979, in van Horn, H. M., Weidemann, V., eds., *IAU Colloq. 53: White Dwarfs and Variable Degenerate Stars*, p. 377
- Montgomery, M. H., Winget, D. E., 1999, *ApJ*, 526, 976
- Montgomery, M. H., Williams, K. A., Winget, D. E., Dufour, P., De Gennaro, S., Liebert, J., 2008, *ApJ*, 678, L51
- Morgan, J. S., Burgett, W., Onaka, P., 2014, in *Society of Photo-Optical Instrumentation Engineers (SPIE) Conference Series*, vol. 9145 of *Society of Photo-Optical Instrumentation Engineers (SPIE) Conference Series*, p. 0
- Mukadam, A. S., et al., 2004, *ApJ*, 607, 982
- Mullally, F., Winget, D. E., Degennaro, S., Jeffery, E., Thompson, S. E., Chandler, D., Kepler, S. O., 2008, *ApJ*, 676, 573
- Nitta, A., et al., 2009, *ApJ*, 690, 560
- Nordhaus, J., Wellons, S., Spiegel, D. S., Metzger, B. D., Blackman, E. G., 2011, *Proceedings of the National Academy of Science*, 108, 3135
- Orosz, J. A., Wade, R. A., 1999, *MNRAS*, 310, 773
- Parsons, S. G., et al., 2015, *MNRAS*, 449, 2194
- Reid, I. N., Liebert, J., Schmidt, G. D., 2001, *ApJ*, 550, L61
- Robinson, E. L., 1979, in van Horn, H. M., Weidemann, V., eds., *IAU Colloq. 53: White Dwarfs and Variable Degenerate Stars*, p. 343
- Rocchetto, M., Farihi, J., Gänsicke, B. T., Bergfors, C., 2015, *MNRAS*, 449, 574
- Romero, A. D., Córscico, A. H., Althaus, L. G., Kepler, S. O., Castanheira, B. G., Miller Bertolami, M. M., 2012, *MNRAS*, 420, 1462
- Sako, M., et al., 2008, *AJ*, 135, 348
- Schmidt, G. D., Smith, P. S., 1995, *ApJ*, 448, 305
- Schmidt, G. D., et al., 2003, *ApJ*, 595, 1101
- Sesar, B., et al., 2007, *AJ*, 134, 2236
- Sorahana, S., Yamamura, I., Murakami, H., 2013, *ApJ*, 767, 77
- Steele, P. R., Burleigh, M. R., Farihi, J., Gänsicke, B. T., Jameson, R. F., Dobbie, P. D., Barstow, M. A., 2009, *A&A*, 500, 1207
- Tout, C. A., Wickramasinghe, D. T., Liebert, J., Ferrario, L., Pringle, J. E., 2008, *MNRAS*, 387, 897
- Tremblay, P.-E., Bergeron, P., Gianninas, A., 2011, *ApJ*, 730, 128
- Voss, B., Koester, D., Østensen, R., Kepler, S. O., Napiwotzki, R., Homeier, D., Reimers, D., 2006, *A&A*, 450, 1061
- Walton, N., 2014, in Wozniak, P. R., Graham, M. J., Mahabal, A. A., Seaman, R., eds., *The Third Hot-wiring the Transient Universe Workshop*, p. 41
- Warner, B., 1995, *Cataclysmic Variable Stars*, Cambridge University Press, Cambridge
- Wickramasinghe, D. T., Ferrario, L., 2000, *PASP*, 112, 873
- Wilson, D. J., Gänsicke, B. T., Koester, D., Raddi, R., Breedt, E., Southworth, J., Parsons, S. G., 2014, *MNRAS*, 445, 1878
- Wilson, D. J., Gänsicke, B. T., Koester, D., Toloza, O., Pala, A. F., Breedt, E., Parsons, S. G., 2015, *MNRAS*, 451, 3237
- Winget, D. E., Kepler, S. O., 2008, *ARA&A*, 46, 157
- Winget, D. E., Robinson, E. L., Nather, R. D., Fontaine, G., 1982, *ApJ Lett.*, 262, L11
- Winget, D. E., et al., 1991, *ApJ*, 378, 326
- Winget, D. E., et al., 2003, in Deming, D., Seager, S., eds., *Scientific Frontiers in Research on Extrasolar Planets*, vol. 294 of *Astronomical Society of the Pacific Conference Series*, p. 59
- Woudt, P. A., Warner, B., Zietsman, E., 2012, *MNRAS*, 426, 2137
- Xu, S., Jura, M., 2014, *ApJ Lett.*, 792, L39